

## Self-consistent effective-mass theory for intralayer screening in graphite intercalation compounds

D. P. DiVincenzo and E. J. Mele

*Department of Physics, University of Pennsylvania, Philadelphia, Pennsylvania 19104-3859*

(Received 3 October 1983)

The effective-mass-approximation differential equations appropriate for impurities in a graphite host are constructed and are used to solve self-consistently for the screening response surrounding a single intercalant atom. The screening cloud is found to have a very slow algebraic decay with a characteristic length of 3.8 Å in the case studied. This rather long length is due to both the semimetallic and the two-dimensional character of graphite. A Thomas-Fermi description of screening is found to be adequate, but a linear-response theory is not. From these results we conclude that the transferred charge in alkali-metal-graphite intercalation compounds is distributed nearly homogeneously on a carbon plane. We discuss recent theoretical and experimental work in light of these results.

### I. INTRODUCTION

The formation of graphite intercalation compounds is believed always to be accompanied by a charge transfer to or from the carbon host. An understanding of the distribution of this excess charge is intimately connected with the understanding of a variety of important physical properties of these compounds: electrical conductivity, the existence of thermodynamically stable staged phases, the dynamics of compound formation, and ionic mobilities. In several intercalation compounds (e.g., AsF<sub>5</sub>-intercalated graphite) a chemical disproportionation associated with a strong in-plane inhomogeneity in the transferred charge is believed to be an important driving force in their stabilization;<sup>1</sup> in fact, this disproportionation has been speculated to drive a charge-density wave in the transferred charge.<sup>2</sup> The in-plane structure of the excess charge in the simpler alkali-metal-graphite intercalation compounds has not been firmly established; some experimental studies<sup>3</sup> suggest that this charge is strongly localized on the C atoms nearest the intercalant, while others<sup>4</sup> support the point of view that the transferred charge is delocalized and hence quite homogeneous.

In this paper we present a new theoretical approach which is well adapted to the calculation of in-plane charge distributions in graphite intercalation compounds. Our approach centers on the use of the effective-mass approximation for the graphite electrons. While an effective-

mass description of the graphite energy bands has been available for some time,<sup>5</sup> it has not previously been applied to the study of electron dynamics in the vicinity of an impurity. The resulting effective-mass-approximation differential equations turn out to be quite different from those for other semimetals.<sup>6</sup> While they bear some resemblance to the multiband equations appropriate for acceptors in semiconductors,<sup>7</sup> the symmetry of the present case allows a dramatic simplification which makes the computation of the screening charge quite straightforward. We find that in the dilute limit (see Fig. 1) a typical alkali-metal donor creates a screening charge which is quite long ranged, decaying algebraically with an effective screening length of about 3.8 Å. This is a direct consequence of the reduced dimensionality of the graphite host, and of the low density of states near the Fermi energy. In addition, we find that the screening is highly nonlinear, being strongly dependent on the valence of the intercalant; in fact, we will show that there is no regime in which a linear-response theory is applicable. We also compare our results with the screening described by Thomas-Fermi theory. This approach, which has been successfully used to predict the layer-averaged excess charge density in higher-stage compounds,<sup>8</sup> compares favorably with our effective-mass-approximation results in the calculation of in-plane screening. The effective-mass theory is superior to the Thomas-Fermi theory, however, in that it also provides information about the eigenstates in the presence of a defect, which should, for example, be useful in future spectroscopic studies. At the same time, the effective-mass approach avoids the excessive computational effort required for a full quantum-mechanical calculation,<sup>9</sup> and is easier to interpret. We believe that the model presented here should thus be applicable to a variety of problems in the electronic structure of intercalation compounds in the future.

The remainder of this paper is organized as follows. Section II develops the formalism of the effective-mass calculation, with a discussion of the construction of a self-consistent screening solution. Section III presents the

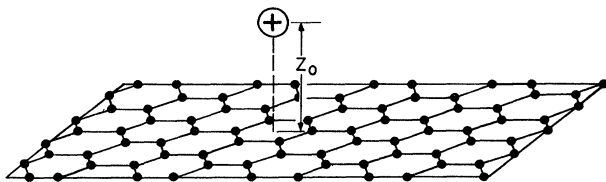


FIG. 1. Model geometry used in the present work: a single, ionized impurity a distance  $z_0$  above an isolated two-dimensional graphite plane.

results of both the effective-mass and the Thomas-Fermi models for a single isolated intercalant in the vicinity of a graphite plane as shown in Fig. 1. Section IV discusses our results in light of several recent experiments on C core spectroscopies in alkali-metal—intercalated graphite compounds. We also mention the implications of the present work for our previous density-functional studies of binding in these compounds. The Appendix develops some mathematical details of the asymptotic decay of the screening charge both in the effective-mass theory and in the Thomas-Fermi model.

## II. THEORY

We have chosen to study the screening of a single intercalant within a graphite host with effective-mass theory.<sup>10</sup> This theory is valid when (i) the major influence of the foreign species on the electronic spectrum occurs near the Fermi level  $E_F$ , and (ii) the resulting disturbance of the host eigenstates is smoothly varying in space, with a length scale much greater than that of the unit cell. The first condition implies that no new chemical bonds are formed between the intercalant and host, and that there are no filled intercalant states. We believe that several intercalants in graphite, in particular the alkali metals, satisfy these conditions. The application of effective-mass theory is slightly different than for the classic semiconductor cases<sup>7</sup> since graphite is a zero-band-gap host; thus the effect on the valence and conduction bands must be considered simultaneously and on the same footing. For this reason we will present the construction of the effective-mass-approximation equations in some detail.

As shown in Fig. 1, we take a two-dimensional (2D) approximation for the graphite host. Within this approximation the host-energy-band structure is quite simple. Figure 2 shows this structure (after Painter and Ellis<sup>11</sup>) for the  $p_\pi$  bands, i.e., states which are odd under basal plane reflection. The valence and conduction bands touch only at the  $K$  point in the Brillouin zone; the effective-mass expansion will be based upon the two degenerate Bloch eigenstates  $\psi_1^S(K, \vec{r})$  and  $\psi_2^S(K, \vec{r})$  at this wave vector. The amplitudes of these two eigenstates are shown in Fig. 3 for a minimal tight-binding model (one  $p_\pi$  orbital per C atom); as shown, we have chosen these eigenstates to lie entirely on one C sublattice or the other, although any rotation in the twofold degenerate subspace is also possible.

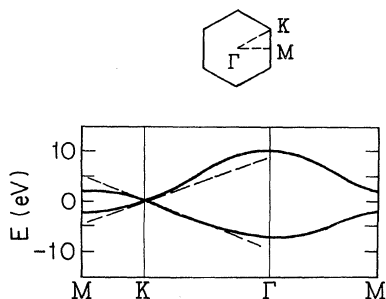


FIG. 2. Energy-band structure of the bands of a two-dimensional graphite layer (Ref. 11). The Brillouin zone is shown above, and the model  $\vec{k} \cdot \vec{p}$  energy bands which form the basis of our effective-mass study are shown as dashed lines.

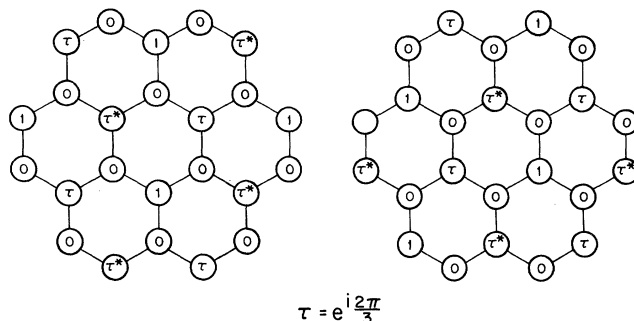


FIG. 3. Two degenerate eigenstates which provide the basis set for the  $\vec{k} \cdot \vec{p}$  trial wave function. The coefficients for a one-orbital description of these eigenstates are shown. They are the two Bloch functions at  $E=0$  at the  $K$  point (see Fig. 2).

When the defect (i.e., intercalant) potential is zero, the effective-mass expansion is equivalent to the  $\vec{k} \cdot \vec{p}$  expansion of the graphite energy bands about  $K$ . We will present the  $\vec{k} \cdot \vec{p}$  results both to introduce the type of wave-function expansion to be used and to illustrate the approximations which are implicitly made to the  $\pi$ -band structure of Fig. 2. In  $\vec{k} \cdot \vec{p}$  theory we approximate the wave function at wave vector  $\vec{k} = K + \vec{\kappa}$  by<sup>11</sup>

$$\psi(\vec{k}, \vec{r}) = f_1(\vec{\kappa}) e^{i\vec{\kappa} \cdot \vec{r}} \psi_1^S(K, \vec{r}) + f_2(\vec{\kappa}) e^{i\vec{\kappa} \cdot \vec{r}} \psi_2^S(K, \vec{r}). \quad (1)$$

Inserting  $\psi$  into the Schrödinger equation, keeping terms of order  $\vec{\kappa}$ , and taking  $E_F=0$  gives the secular equation,

$$\frac{\hbar}{m} \vec{\kappa} \cdot \begin{bmatrix} \vec{p}_{11} & \vec{p}_{12} \\ \vec{p}_{21} & \vec{p}_{22} \end{bmatrix} \begin{bmatrix} f_1(\vec{\kappa}) \\ f_2(\vec{\kappa}) \end{bmatrix} = E(\vec{\kappa}) \begin{bmatrix} f_1(\vec{\kappa}) \\ f_2(\vec{\kappa}) \end{bmatrix}. \quad (2)$$

Here  $\vec{p}_{ij} \equiv \int \psi_1^{S*}(K, \vec{r}) \vec{p} \psi_j^S(K, \vec{r}) d\vec{r}$ . It can be shown from group-theoretic arguments (and we can verify directly within the one-orbital tight-binding model) that the momentum matrix may be written in the form

$$\vec{p} \begin{bmatrix} 0 & \hat{x} - i\hat{y} \\ \hat{x} + i\hat{y} & 0 \end{bmatrix}. \quad (3)$$

$\hat{x}$  and  $\hat{y}$  are basal-plane unit vectors, and  $\vec{p}$  is a number related to the bandwidth (see below). With the use of Eq. (3) (2) is very easily diagonalized to give

$$E(\kappa) = \pm P |\vec{\kappa}|, \quad (4)$$

where  $P \equiv (\hbar/m)\vec{p}$ . Thus the essence of the  $\vec{k} \cdot \vec{p}$  approximation (and also of the effective-mass theory) is to replace the graphite bands by conical dispersions at  $E_F$  (see Fig. 3).

When an external circularly symmetric potential  $U(r)$  is imposed, translational symmetry is broken and the eigenfunctions can no longer be labeled by  $\vec{\kappa}$ . This requires a slight generalization of the trial wave function (1),

$$\psi(\vec{r}) = \int d\vec{\kappa} f_1(\vec{\kappa}) e^{i\vec{\kappa} \cdot \vec{r}} \psi_1^S(K, \vec{r}) + \int d\vec{\kappa} f_2(\vec{\kappa}) e^{i\vec{\kappa} \cdot \vec{r}} \psi_2^S(K, \vec{r}). \quad (5)$$

Inserting this trial wave function into the Schrödinger equation leads to an integral equation

$$P \begin{pmatrix} 0 & \kappa'_x - i\kappa'_y \\ \kappa'_x + i\kappa'_{0y} & 0 \end{pmatrix} \begin{pmatrix} f_1(\vec{\kappa}') \\ f_2(\vec{\kappa}') \end{pmatrix} + \int d\vec{\kappa} U_2(\vec{\kappa}' - \vec{\kappa}) \begin{pmatrix} f_1(\vec{\kappa}) \\ f_2(\vec{\kappa}) \end{pmatrix} = E \begin{pmatrix} f_1(\vec{\kappa}') \\ f_2(\vec{\kappa}') \end{pmatrix}. \quad (6)$$

Here

$$U_2(q) = \int dz \bar{\rho}(z) U(q, z) = \int dz \bar{\rho}(z) \left[ \int d\vec{q} e^{-i\vec{q}\cdot\vec{r}} U(r) \right].$$

$U_2$  is the 2D Fourier transform of the defect potential  $U(r)$ , averaged over the  $\pi$  charge density profile  $\bar{\rho}(z)$ . In arriving at Eq. (6) we have made the standard approximation of effective-mass theory<sup>12,13</sup> that the defect potential is short ranged in  $\vec{q}$  space, i.e.,  $U_2(\vec{G}) \approx 0$ , where  $\vec{G}$  is the shortest nonzero reciprocal-lattice vector of the graphite plane. In real space this implies that  $U(r)$  varies smoothly from one unit cell to the next; this will be verified below. The short-range character of  $U_2$  in reciprocal space also permits us to assume that there is no "intervalley scattering" between equivalent  $K$  points in the graphite Brillouin zone.<sup>7</sup>

To complete the derivation, we convert Eq. (6) from an integral to a differential equation by Fourier transformation in  $\vec{\kappa}$ :

$$\frac{P}{i} \begin{pmatrix} 0 & \frac{\partial}{\partial x} - i\frac{\partial}{\partial y} \\ \frac{\partial}{\partial x} + i\frac{\partial}{\partial y} & 0 \end{pmatrix} \begin{pmatrix} F_1(\vec{r}) \\ F_2(\vec{r}) \end{pmatrix} = [E - U_2(r)] \begin{pmatrix} F_1(\vec{r}) \\ F_2(\vec{r}) \end{pmatrix}. \quad (7)$$

From (5), the trial wave function is now expressed as

$$\psi(\vec{r}) = F_1(\vec{r}) \psi_1^S(K, \vec{r}) + F_2(\vec{r}) \psi_2^S(K, \vec{r}),$$

i.e., as smoothly varying envelope functions  $F_i(\vec{r})$  multiplying graphite Bloch functions. Note that this trial function is incapable of describing covalent bonding between the defect and host, nor can it describe an eigenstate located on the defect; however, it is well adapted to describe certain intercalation systems (e.g., Li-intercalated graphite) in which charge transfer is complete and host-defect interaction is weak. In what follows we will make a sheet approximation to the graphite plane and take  $\bar{\rho}(z) = \delta(z)$ . No essential modifications are required to relax this assumption.

We will rely on the solutions of Eq. (7) for a description of graphite electron dynamics in the vicinity of an impurity. We can simplify these solutions and gain insight into their behavior by exploring some of the mathematical properties of the differential equation (7). First we rewrite it in a canonical form,

$$\left[ \frac{P}{i} \vec{\sigma} \cdot \vec{\nabla} + U_2(r) - E \right] \Psi(\vec{r}) = 0. \quad (8)$$

Here  $\vec{\sigma} \cdot \vec{\nabla}$  represents the two-dimensional dot product  $\sigma_x(\partial/\partial x) + \sigma_y(\partial/\partial y)$ , where  $\sigma_x$  and  $\sigma_y$  are conventional  $2 \times 2$  Pauli matrices.<sup>14</sup> Since the Pauli matrices anticommute, Eq. (8) is algebraically identical to a two-dimensional Dirac equation,<sup>15</sup> where the two-component "spinor" wave function  $\Psi$  does not represent "spin up" and "spin down," but rather "graphite sublattice 1" and "graphite sublattice 2." The effective "speed of light" in Eq. (8) is proportional to  $v_F$  which we have chosen to match the energy-band dispersion of graphite near  $E_F$  (Ref. 11) and has a value  $P = \hbar v_F = 5.39$  eV Å. Also, for the Dirac effective mass in (8)  $m^* = 0$ , since the two bands touch.

The primary importance of this identification with the Dirac equation is that it immediately permits us to construct the azimuthal parts of the spinor wave function. We start with the observation that the operator,

$$J_z = L_z + \frac{1}{2} \sigma_z = \begin{pmatrix} xp_y - yp_x + \frac{1}{2} & 0 \\ 0 & xp_y - yp_x - \frac{1}{2} \end{pmatrix},$$

commutes with the Hamiltonian of Eq. (8) if  $U(r)$  has circular symmetry, which we assume.  $J_z$  is of course formally identical to the total angular momentum in a Dirac system, although it is not directly related to the real angular momentum of the graphite eigenstates. The eigenvalues of  $J_z$  are half-integer and doubly degenerate, with the eigenspinors of  $j = m + \frac{1}{2}$  given by  $(e^{im\vartheta}, 0)^T$  and  $(0, e^{i(m+1)\vartheta})^T$ . The eigenspinor of Eq. (8) with azimuthal quantum number  $j$  must therefore be some combination of these two:

$$\Psi = \begin{pmatrix} -i\sqrt{2}a(r)e^{im\vartheta} \\ \sqrt{2}b(r)e^{i(m+1)\vartheta} \end{pmatrix} \quad (9)$$

(the prefactors are arbitrary and are chosen for later convenience). Substitution of (9) into (8) leads to coupled ordinary differential equations for  $a(r)$  and  $b(r)$  (Ref. 16):

$$\begin{aligned} \frac{da(r)}{dr} - \frac{m}{r}a(r) &= -\frac{E - U_2(r)}{P}b(r), \\ \frac{db(r)}{dr} + \frac{m+1}{r}b(r) &= \frac{E - U_2(r)}{P}a(r). \end{aligned} \quad (10)$$

Equations (10) lend themselves to a very straightforward numerical solution. Because the spectrum has no gap, i.e.,  $m^* = 0$ , (10) has no bound states and solutions match onto continuum states at all energies. These continuum solutions are simple phase-shifted free-particle solutions, which are ordinary Bessel functions:

$$\begin{aligned}
 a_j(r \rightarrow \infty) &= C \left[ \cos \delta_j J_m \left[ \frac{|E|r}{P} \right] - \sin \delta_j N_m \left[ \frac{|E|r}{P} \right] \right], \\
 b_j(r \rightarrow \infty) &= \pm C \left[ \cos \delta_j J_{m+1} \left[ \frac{|E|r}{P} \right] - \sin \delta_j N_{m+1} \left[ \frac{|E|r}{P} \right] \right].
 \end{aligned} \tag{11}$$

Here  $\pm$  pertains to  $E > 0$  and  $E < 0$ , respectively. The normalization constant  $C$  may be determined if we make the following identification of the charge density from the effective-mass trial wave function:

$$\rho(\vec{r}, E) = \sum_{j=-\infty}^{\infty} (|F_{1j}(\vec{r}, E)|^2 + |F_{2j}(\vec{r}, E)|^2). \tag{12}$$

Equation (12) ignores the actual atomic level variations in  $\rho$  arising from the Bloch function  $|\psi_j^S(K, \vec{r})|^2$ ; this is in the spirit of the effective-mass theory. Equation (12) should also contain cross terms, but these integrate to zero in each unit cell and we will ignore them as well.  $|F_1|^2$  and  $|F_2|^2$  may be viewed as the envelope of the charge densities on the two graphite sublattices. These envelopes are actually identical after  $j$  summation because of the symmetry between  $+j$  and  $-j$  solutions:

$$\begin{aligned}
 a_{(-j)}(r) &= b_j(r), \\
 b_{(-j)}(r) &= -a_j(r).
 \end{aligned}$$

Given Eq. (12), we can fix  $C$  by requiring that the correct density of states be obtained for  $U_2 = 0$ :

$$\rho(E) \equiv \frac{1}{A} \int_A d\vec{r} \rho(\vec{r}, E) = \frac{2|E|}{\pi P^2}. \tag{13}$$

This gives  $C = 1/P(|E|/2\pi)^{1/2}$ .

Even prior to any detailed numerical calculations, a general understanding of graphite's response to an external potential may be obtained by considering some of the general properties of the scattering phase shifts of Eq. (11). It can be shown quite generally from the small argument behavior of the Bessel functions that  $\delta_j \rightarrow 0$  as  $|E| \rightarrow 0$  for any  $j$ . The behavior of  $\delta_{1/2}$  near  $E = 0$  is, however, quite pathological:

$$\delta_{1/2} \cong \frac{\pi}{2 \ln(|E|r_s/2P)}. \tag{14}$$

Here  $r_s$  is a characteristic length scale for the defect potential  $U_2$ . Otherwise, Eq. (14) has no dependence on the detailed form of  $U_2$ ; it is even insensitive to  $U_2$ 's sign. This lowest-order behavior of the phase shift permits us to deduce the long-range behavior of the induced charge density in the presence of an impurity. Using an analysis akin to that used to compute conventional Friedel oscillations,<sup>17</sup> we find

$$\Delta\rho(r) \propto \int_0^{\infty} \frac{1}{r} \sin[\delta_{1/2}(E)] \sin\left[\frac{2|E|r}{P}\right] dE. \tag{15}$$

This integral may be performed by the method of steepest descents; we will not show the details here. The result is

$$\Delta\rho(r \rightarrow \infty) = -\frac{f(r)}{r^2}. \tag{16}$$

Here  $f(r)$  is a rather complicated but slowly varying function of  $r$  which goes to zero logarithmically as  $r \rightarrow \infty$ . Further details of the mathematics leading to this result are given in the Appendix. This result differs from ordinary Friedel oscillations in several respects: (i) Since the system is two dimensional, the characteristic power-law falloff is  $r^{-2}$  rather than  $r^{-3}$ . Still, like the Friedel charge density Eq. (16) is just barely integrable, made so only by the behavior of  $f(r)$ . To this extent we are justified in our original point of view that the influence of a defect is very long ranged in graphite. (ii) Equation (16) is not oscillatory, but goes monotonically to zero in the asymptotic region. This is understandable since graphite has  $k_F = 0$ , so that the "oscillation wavelength" is infinite. (iii) As mentioned above, the sign of (16) is independent of the sign of  $U_2(r)$ ; charge is depleted at long distance, no matter what the ionicity of the defect may be.

A further analysis of the phase-shift properties of Eq. (10) uncovers an important flaw in the effective-mass approximation for graphite. A study of  $\delta_j(E \rightarrow -\infty)$  reveals that the phase shift at  $-\infty$  does not go to an integer multiple of  $\pi$ ; Levinson's theorem<sup>18</sup> is thus not satisfied in this system. In fact, this asymptotic phase shift depends on the details of the defect potential. For example, for a square-well potential

$$U_2(r) = \begin{cases} V, & r < r_c \\ 0, & r \geq r_c \end{cases}.$$

$\delta_j(E \rightarrow -\infty) \rightarrow Vr_c/p$  independent of  $j$ . This demonstrates that the present theory possesses the undesirable property that an important physical requirement, the Friedel rule,<sup>17</sup>

$$Z = (2/\pi) \sum_j [\delta_j(0) - \delta_j(-\infty)], \tag{17}$$

can never be satisfied since the right-hand side of Eq. (17) is infinite. ( $Z$  is the valence of the impurity.) This result is true no matter what the form of  $U_2(r)$ . The cause for this unphysical behavior is that in the model the valence band extends to  $E = -\infty$  and contains an infinite amount of charge. The real graphite  $\pi$  band, of course, has a finite bandwidth and contains a single electron per C atom. This suggests a simple *ad hoc* correction to the effective-mass model in which we simply impose a lower cutoff  $E_c$  on the effective-mass density of states, with  $E_c$  chosen to give the correct average charge density of  $\pi$  electrons. This is essentially the scheme which we have adopted, with two improvements. (i) In the spirit of Thomas-Fermi theory, we take the lower band edge to vary spatially according to the strength of the external potential:  $E_c(r) = E_c^0 + U_2(r)$ . (ii) The band edge is taken to be gradual rather than abrupt. This reduces spurious Friedel-type oscillations arising from the band minimum. This

scheme is embodied in the following formula for the total induced charge density  $\Delta\rho(r)$ :

$$\Delta\rho(r) = \int_{-\infty}^0 [f(E - U_2(r))\rho(r, E) - f(E)\rho^0(r, E)] dE. \quad (18)$$

Here  $\rho(r, E)$  is defined by Eq. (12), with  $\rho^0$  denoting the no defect charge density.  $f(E)$  is the smooth cutoff function

$$f(E) = \begin{cases} 0, & E < E_c^0 - \delta E \\ \frac{E - E_c^0 + \delta E}{\delta E}, & E_c^0 - \delta E < E < E_c^0 \\ 1, & E > E_c^0 \end{cases}. \quad (19)$$

$E_c^0 = -4.3$  and  $\delta E = 3.0$  eV were chosen to match the graphite  $\pi$  charge density. All the numerical results presented below for the effective-mass model use the scheme of Eqs. (18) and (19). Actually, a much more desirable scheme is to permit the eigenstates in the presence of the defect to be constructed only from defect-free eigenstates lying within the energy range  $E_c^0 < E < -E_c^0$ . In this way the spurious states for  $E \rightarrow -\infty$  would be very naturally projected out. Unfortunately, we judged this approach to be too cumbersome for practical calculation. The procedure described by Eqs. (18) and (19) mimics this projection. Within this scheme the majority of screening effects arises from states near the Fermi energy rather than deep in the band, as is physically reasonable. Still, this procedure has some small deficiencies which limit its applicability to some extent, as we shall describe below.

Finally, we explain our construction of the defect potential  $U_2(r)$ . It contains two parts:<sup>19</sup>

$$U_2(r) = U_2^{\text{ext}}(r) + U_2^H(r). \quad (20)$$

We take  $U_2^{\text{ext}}(r)$  to be the potential of a point ion situated a distance  $z_0$  above the graphite plane, as seen in the basal plane [see the comment below Eq. (7)]:

$$U_2^{\text{ext}}(r) = \frac{Ze^2}{(z_0^2 + r^2)^{1/2}}. \quad (21)$$

$U_2^H(r)$  is the electrostatic potential in the basal plane generated by the charge sheet  $\Delta\rho(r)$  of Eq. (18):

$$U_2^H(r) = e^2 \int \frac{\rho(\vec{r}') d\vec{r}'}{|\vec{r} - \vec{r}'|} = \frac{e^2}{\pi} \int e^{-i\vec{q} \cdot \vec{r}} \frac{\Delta\rho(q)}{|\vec{q}|} d\vec{q}, \quad (22)$$

where  $\Delta\rho(q)$  is the 2D Fourier transform of Eq. (18) obtained by a fast Fourier-Bessel algorithm.<sup>20</sup> We perform an iterative computation of Eqs. (10), (12), (18), and (20)–(22) until the potential and charge density are self-consistent. No exchange interactions are included in the present model.

### III. RESULTS

In this section we give results of a numerical evaluation of the equations described above for a single impurity placed  $z_0 = 2.7$  Å above a graphite plane (see Fig. 1). For

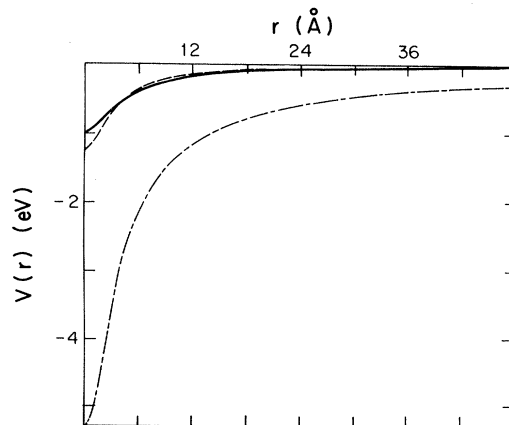


FIG. 4. Self-consistent defect potential  $U_2(r)$  for  $Z = +1$  and  $z_0 = 2.7$  Å. The solid line is the effective-mass result, the dashed line the Thomas-Fermi result. Note the strong similarity between them. The dotted-dashed line shows the bare defect potential.

most of the results presented below, the valency of the impurity is taken as  $Z = \pm 1$ .

Figure 4 shows our results for the induced potential  $U_2(r)$ . Here the solid curve shows  $U_2$  for our effective-mass theory, the dotted-dashed curve is the unscreened impurity potential, and the dashed line is the result of a Thomas-Fermi screening calculation to be described below. These results may be understood by noting that the potential must fall between two limits. If the electrons behave classically (that is, if the electronic kinetic energy is irrelevant to the total energy minimization) then the electrons will form a classical image charge in the basal plane. The graphite potential thus becomes an equipotential surface, and  $U_2^{\text{cl}}(r) = 0$ . The image charge is thus one limit; the real charge density cannot be more localized than the classical image charge, i.e., the actual  $U_2(r)$  cannot be greater than zero. The other extreme is achieved by a system in which the electronic kinetic energy is so great that the electrons are incapable of responding to the external potential and form no screening cloud. In this case  $U_2^{\text{OM}}(r) = U_2^{\text{ext}}(r)$ , which is shown as the dotted-dashed line in Fig. 4. The actual result for  $U_2(r)$  from the effective-mass model, shown by the solid line in Fig. 4, is intermediate between the two limiting cases, indicating that electron kinetic and potential energies are playing roughly equal roles in the screening process. The actual  $U_2(r)$  continues to have an algebraically decaying tail, indicative of the long-range response of the graphite plane. In Fig. 4 we have also compared the effective-mass result with the  $U_2(r)$  obtained using Thomas-Fermi theory (dashed line). This theory, which has been applied previously to other graphite systems with slightly different geometries,<sup>8</sup> is based on a spatially varying assignment of the Fermi energy,

$$E_F(r) = -U_2(r). \quad (23)$$

The local charge density is then identified [using Eq. (13)] as

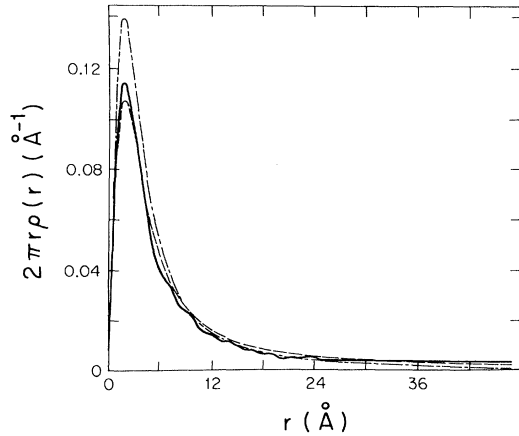


FIG. 5. Screening charge density  $\Delta\rho(r)$  multiplied by the volume element  $2\pi r$  for a defect with  $Z = +1$ ,  $z_0 = 2.7$  Å. Again, the solid line is the effective-mass result, the dashed line the Thomas-Fermi result. Note the long tail on both of them. The dotted-dashed line is the classical image charge.

$$\Delta\rho(\vec{r}) = \int_0^{E_F(\vec{r})} \rho(E) dE = \frac{-[U_2(r)]^3}{|U_2(r)| \pi P^2}. \quad (24)$$

The dashed curve in Fig. 4 is a result of an iterative solution of Eq. (24) along with the Poisson equation, Eqs. (20)–(22). The effective-mass and the Thomas-Fermi results are seen to agree rather closely. This is not entirely unexpected, given that the Thomas-Fermi approximation should be adequate when the disturbance is slowly varying in space. Still, the quantitative agreement is somewhat surprising, and implies that Thomas-Fermi theory is very useful in examining broad trends in this system. We will give an example of this sort of analysis below.

Figure 5 shows the induced charge density  $\Delta\rho(r)$  generated by  $U_2$  of Fig. 4. Again, the effective-mass result is shown as a solid line and the Thomas-Fermi result as a dashed line. The strong similarity between them is again evident. Within the Thomas-Fermi approximation, we can compute the asymptotic behavior of  $\Delta\rho(r)$  as  $r \rightarrow \infty$ . The result is

$$\Delta\rho(r) = \pm \frac{g(r)}{r^2}, \quad (25)$$

where  $g(r)$  is a slowly varying function which goes logarithmically to zero as  $r \rightarrow \infty$ , as in Eq. (16). [Consult the Appendix for the derivation of Eq. (25).]

The Thomas-Fermi and effective-mass solutions thus have almost the same asymptotic dependence at large  $r$ . However, one important difference is that while the effective-mass result is independent of the sign of  $U_2(r)$  for large  $r$ , the Thomas-Fermi result follows the sign of  $U_2$ . [This is the meaning of the  $\pm$  in Eq. (25).] For  $Z > 0$ , this means that the two results for  $\Delta\rho(r)$  should have opposite signs at long distance. In Fig. 5 they have the same sign. This is probably a result of a deficiency in the numerical calculation of the effective mass  $\Delta\rho(r)$ ; it is difficult to reproduce numerically the rather delicate logarithmic phase-shift singularity of Eq. (14) for  $E \rightarrow E_F$ . Still, we expect that the computation is reliable in the

physically relevant “large” region, i.e.,  $0 < r \lesssim 30$  Å.

Figure 5 also shows the  $\Delta\rho(r)$  for the image-charge model. This charge density is simply

$$\Delta\rho^{\text{im}}(r) = \frac{1}{2\pi} \frac{z_0}{(z_0^2 + r^2)^{3/2}}. \quad (26)$$

As described earlier, the correct charge density is much smaller near the defect than the image charge (see Fig. 5). In addition, the effective-mass charge density has a much more diffuse tail at large  $r$  ( $\sim 1/r^2$ ) than the image charge ( $\sim 1/r^3$ ). We would like to summarize these facts by a single number which characterizes the effective screening length  $\lambda$ . One possible definition of  $\lambda$  is the first moment of  $\Delta\rho(r)$ :

$$\lambda = \int_0^\infty r \Delta\rho(\vec{r}) d\vec{r}. \quad (27)$$

This is not a useful definition, since it is divergent for both the effective mass  $\Delta\rho(r)$  and the image model  $\Delta\rho^{\text{im}}(r)$ . We therefore choose to define  $\lambda$  in a way which is related to the median of the charge distribution:

$$\int_0^{\sqrt{3}\lambda} \rho(\vec{r}) d\vec{r} = \frac{Z}{2}. \quad (28)$$

The  $\sqrt{3}$  factor is chosen such that for the image charge,  $\lambda = z_0 = 2.7$  Å. Then using Eq. (28) for the effective mass or Thomas-Fermi  $\Delta\rho(r)$  we find  $\lambda \simeq 3.8$  Å. Thus by this measure (and, we suspect, by any other reasonable measure which could be invented) the screening length is about 50% larger than an image-charge theory would predict. Note that we have not included any background dielectric response for the graphite electrons; if we had, the predicted would be somewhat larger. We have thus demonstrated that graphite, because of its semimetallic electronic structure, screens much less efficiently than an ideal metal, even a two-dimensional one. It is also interesting to note that Ref. 8, in a Thomas-Fermi model for screening perpendicular to graphite planes, found a very similar screening length,  $\lambda = 4$  Å, despite the different geometry and some differences in the definition of  $\lambda$ . We will explore the implications of this result for intercalation compounds of graphite in Sec. IV.

Another consequence of the unusual electronic structure of graphite is the dependence of the screening on the valency of the defect  $Z$ . Figure 6 shows the dependence on  $Z$  of the self-consistent potential at the origin. This curve has been generated numerically via the Thomas-Fermi approach. The Thomas-Fermi theory has exact  $Z \rightarrow -Z$  symmetry. The effective-mass model, on the other hand, does not have this exact symmetry; nevertheless, the effective-mass results are nearly  $\pm Z$  symmetric, and they lie close to the Thomas-Fermi curve for  $|Z| \sim 1$ , confirming the similarity of the two models. For  $|Z| \ll 1$  the effective-mass points lie well below the curve in Fig. 6. This results from our valence-band cutoff procedure, Eqs. (18) and (19). When  $|Z|$  becomes small, the small screening effects which we wish to study near  $E_F$  are masked by numerical noise in the cutoff procedure at the bottom of the band. For this reason, it is more appropriate to use the Thomas-Fermi calculation to study the general trends of the screening potential.

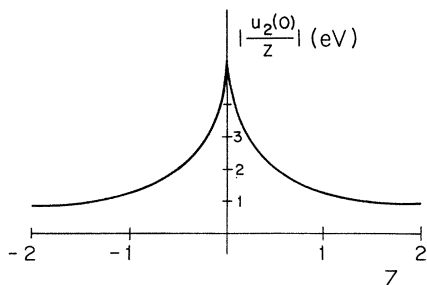


FIG. 6. Total potential  $U_2(r)$  at  $r=0$ , divided by the defect valency  $Z$ , as a function of  $Z$ . This curve has been computed in the Thomas-Fermi model, and shows the nonlinearity of the response with  $Z$ . The cusp at the origin is real and demonstrates that linear-response theory is never valid.

The behavior of the curve in Fig. 6 can be understood with some fairly simple arguments. The relative magnitude of the screened potential decreases with increasing  $Z$ ; this means that the screening is becoming more effective (i.e., is approaching the image-charge result in the language of our earlier discussion) because the density of states at  $E_F$  in the vicinity of the defect,  $\rho(E_F(r))$  [see Eqs. (13) and (24)], is becoming larger. It is not clear whether the screening becomes entirely imagelike as  $Z \rightarrow \infty$ ; the curve is falling only gradually towards this limit. In the opposite limit,  $Z \rightarrow 0$ , the density of states at  $E_F$  remains very low. Consequently the screening becomes very ineffective (the "kinetic-energy-dominated" regime discussed above), and  $|U_2(0)/Z| \rightarrow e^2/z_0$ . A study of the Thomas-Fermi equations shows that the curve in Fig. 6 has a genuine cusp at  $Z=0$ , and its derivative is actually undefined at the origin. This result has the important consequence that a linear-response model for impurity screening in graphite is not applicable even for very small impurity potential. This is so because a linear relation between external potential and total potential,  $U_2 \sim \chi U_2^{\text{ext}}$ , would imply that the derivative,

$$\frac{d}{dZ} \left( \frac{|U_2(0)|}{Z} \right)$$

is zero for small  $Z$ . Figure 6 shows that this never happens. The fundamental reason is that  $\rho(E_F)$  can never be assumed to be nearly constant, no matter how small  $Z$  is, since  $\rho(E_F)$  is nonanalytic at  $E_F=0$ . Impurity screening in graphite is thus intrinsically and unavoidably a nonlinear problem.

#### IV. DISCUSSION

In the above section we have presented results for the induced potential and charge density of a single intercalant inside a graphite host. More typically, of course, we are interested in the charge distribution induced by an entire layer of intercalants. We may apply our results to this problem with the zeroth-order approximation that the total charge density or potential is simply a linear superposition of contributions from each separate atom. With this assumption, we find that our model predicts that for an intercalant layer of typical density in a graphite inter-

calation compound (between  $\frac{1}{6}$  and  $\frac{1}{12}$  of an intercalant per C atom), the charge transferred to the graphite layer is quite homogeneously distributed, with only a small enhancement of charge near the intercalants and a small depletion away from them. This is a result of both the large median distance of the induced charge from the impurity, which at 3.8 Å is comparable to the distance between intercalants, as well as of the extended algebraic tail contributed by each charge cloud.

A variety of both theoretical and experimental studies has attempted to quantify the homogeneity of the excess charge density on the graphite planes, with conflicting results. A very reliable and accurate theoretical computation of the in-plane charge distribution of  $\text{LiC}_6$  by Holzwarth *et al.*<sup>9</sup> was capable of showing differences between the charge densities of C-C  $\sigma$  bonds at different distances from a Li intercalant. This study did not examine the in-plane inhomogeneities in the C  $\pi$  states, nor would it have been able to study the dependence of this inhomogeneity on the in-plane Li density. A Huckel study of a model acceptor system<sup>21</sup> has found the transferred charge density to be highly localized on C atoms neighboring the intercalant. However, this study cut off the Hartree interaction at short range, which may well miss the essential physics of the screening. Among the experimental studies, the C 1s x-ray photoemission spectroscopy (XPS) measurements by DiCenzo *et al.*<sup>3</sup> on Li- and K-intercalated graphite deduced the presence of inequivalent C sites by the analysis of the broad asymmetric C 1s line shape. On the basis of the distribution of C 1s binding energies deduced from this line-shape analysis, the authors conclude that the transferred  $\pi$  charge density is highly inhomogeneous, being strongly localized on the nearest-neighbor C atoms to the intercalant. The authors further conclude that the potential energy induced by the presence of the intercalant is more positive for electrons near C nuclei neighboring the intercalant atoms than for those near more-distant C sites. These conclusions are not supported by the present study. Given the strong delocalization of transferred  $\pi$  charge predicted by our theory, we expect that the different C atoms should be only weakly distinguishable according to their 1s binding energy. Furthermore, our model would predict that C atoms closer to the intercalant will lie in a more negative potential well than more distant C atoms rather than the more positive potential deduced in Ref. 3. This follows from our argument that the attractive external ion potential denoted  $U_2^{\text{ext}}$  above can only be incompletely screened by polarization of the graphite  $\pi$  electrons since graphite is a nonideal metal. Thus for intercalated donors the net potential  $U_2$  seen by the C cores must be negative and weakly monotonically increasing with increasing distance from the intercalant. More evidence comes from a recent measurement of the C 1s  $E_F$  energy-loss function<sup>4</sup> for first-stage alkali compounds which indicates that the threshold line shape is not consistent with the proportions of inequivalent C's reported in the XPS study. In addition, a recent <sup>13</sup>C NMR study in a variety of K-intercalated compounds reported<sup>22</sup> only small difference between Knight shifts of C atoms in the same layer. A possible explanation of the XPS data is that the collective response of the

C valence electrons to the 1s core hole in graphite differs from the assumed response of an ordinary 3D metal.<sup>23</sup>

A theoretical study of the 1s energy-loss threshold in stage-1 FeCl<sub>3</sub>-intercalated graphite<sup>24</sup> previously found that the 1s core absorption spectra are strongly influenced by the energy dependence of the graphite empty density of states. We have made a preliminary study of the core exciton problem using the present effective-mass theory. This calculation is identical to the model intercalation problem described above, with  $z_0=0$  (i.e., the perturbing potential in the graphite plane) and  $Z=1$  corresponding to the ionized 1s level. We have also varied  $E_F$  to study the effect of different band fillings of the acceptors and donors on the core spectrum. This approach differs from the lattice model of Ref. 24 in that we compute the Hartree potential of the screening charge, and thus obtain a self-consistent valence-electron response. The core absorption profile (proportional to the square of the upper spinor component of the  $j=\frac{1}{2}$  effective-mass wave functions at  $r=0$ ) again shows substantial excitonic modifications to the line shape. We find a strong difference in the core-hole response between donor and acceptors. Unfortunately, the effective-mass approximation is incapable of making reliable quantitative predictions of these line shapes. This is so because, unlike the impurity screening response, the core-hole response is found to contain a highly localized component, which violates the assumptions of our continuum effective-mass theory. This localization occurs both because the external potential is more localized for  $z_0=0$  than for  $z_0\neq 0$ , and because the host is more metallic when  $E_F\neq 0$ . These results suggest that it would be appropriate to reexamine this problem theoretically using the lattice model of Ref. 24, but with self-consistency effects included. A proper description of the 1s line shape in either absorption or photoemission may also require a consideration of electronic many-body effects beyond the final-state rule<sup>25</sup> and specific to the collective response of the graphite  $\pi$  charge.

Our present calculation is also relevant to our previous study of intercalant-intercalant in-plane binding; we previously found that the effective Coulomb interaction between ions becomes *attractive* at large in-plane lattice constant<sup>26</sup> because of the presence of the transferred charge on the adjoining graphite plane. Further, we find that this Coulomb potential dominates the total potential between Li ions<sup>27</sup> and contributes to a stable minimum in the Li interaction at a lattice constant corresponding to a Li density of approximately LiC<sub>7</sub>. However, these results are contingent on the assumption that the charge density transferred to the C  $\pi$  bands remains nearly homogeneously distributed throughout the range of a physical in-plane lattice constant [e.g.,  $\sqrt{3}\times(2.46 \text{ \AA}) < a_0 < \sqrt{2}\times\sqrt{3}\times(2.46 \text{ \AA})$  for Li-intercalated graphite]. This assumption is justified by the present work, which indicates that inhomogeneities of the in-plane charge density will only have important effects on the Coulomb potential for  $a_0 \gtrsim 4 \text{ \AA}$ . Thus the use of the in-plane interaction which we previously derived in, for example, mean-field studies of intercalant phase diagrams<sup>28</sup> seems to be satisfactory in the region of interest.

The effective-mass approach which we have presented

here provides a particularly elegant and useful mathematical description of a variety of electronic phenomena in graphite intercalation compounds. There are a number of obvious extensions to the work presented here which would be relevant to other problems of present interest. For example, Eq. (8) could accommodate a potential  $U_2(r)$  corresponding to a lattice of impurities; the solution of the effective-mass equations would proceed in the spirit of an ordinary self-consistent band-structure calculation (but would be much more tractable). Such a calculation is important since there are likely to be significant nonlinearities (i.e., departures from the simple superposition rule used above) as a function of intercalant density which result from the dependence of the density of states at  $E_F$  on the charge density. Still, we do not expect to see the strong induced charge-density wave as predicted in the acceptors.<sup>1,2</sup> This calculation could provide the basis for a quantitative discussion of the XPS line shape in alkali-metal-intercalated graphites.<sup>3</sup> A definitive study would include the effects of three dimensionality, and of intervalley and umklapp scattering; systematic procedures for including these exist within the effective-mass framework.<sup>7</sup>

To summarize, we have constructed an effective-mass theory which permits a calculation of many of the electronic properties of alkali-metal-intercalated graphites without the extraordinary labor of the full-band-structure approach. For the single-impurity problem, we find an induced charge density which is much more diffuse than predicted by image-charge theory. This extended response, which is also accurately predicted by Thomas-Fermi theory, results from the reduced dimensionality and the semimetallic band structure of the graphite host. The unusual band structure also causes the corresponding linear-response theory of impurity screening to be invalid under all circumstances. Our calculation supports the point of view that the transferred charge in a typical alkali-metal-intercalated graphite compound is nearly homogeneously distributed on the bounding C planes.

#### ACKNOWLEDGMENTS

We are grateful to Professor P. Soven for his interest and helpful suggestions, and to Professor J. E. Fischer and Dr. D. Allan for their critical reading of this manuscript. This work is supported by the National Science Foundation Materials Research Laboratories Program on Grant No. DMR-82-16718. One of us (E.J.M.) acknowledges the support of a fellowship from the Alfred P. Sloan Foundation.

#### APPENDIX

A very important and surprising result of the present work is that the asymptotic behavior of the screening of a point charge by a graphite layer is  $\Delta\rho(r)\sim 1/r^2$ . This is much slower than  $\Delta\rho(z)\sim 1/z^4$  (Ref. 8) for the screening of a plane of charge embedded in a stack of graphite planes, and it provides a significant contribution to our argument that the screening charge for an array of intercalants is homogeneously distributed on the bounding gra-

phite plane. In this Appendix we present details of the derivation of this result both within the effective-mass theory and the Thomas-Fermi approximation.

To obtain the asymptotic behavior  $\Delta\rho(r) \sim -f(r)/r^2$  in effective-mass theory [Eq. (16) in the text], we return to Eq. (14) for the  $j = \frac{1}{2}$  phase shift near  $E_F = 0$  in the presence of a potential. This may be obtained by using the 2D phase shift formula derived using Eq. (11):

$$\tan\delta_j = \frac{kJ'_m(kr_s) - \gamma_j J_m(kr_s)}{kN'_m(kr_s) - \gamma_j N_m(kr_s)}. \quad (\text{A1})$$

Here  $k \equiv |E|/p$  and the prime indicates a derivative with respect to the argument of the Bessel function. The logarithmic derivatives  $\gamma_j$  may be assumed to vary smoothly in the neighborhood of  $E = 0$ . We also assume that the defect potential  $U_2(r)$  vanishes outside a cutoff radius  $r_s$ . The small- $E$  behavior of the  $j = \frac{1}{2}$  phase shift is obtained by using the small argument expressions for  $J_0$  and  $N_0$ :

$$J_0(x) = 1, \quad J'_0(x) = 0, \quad (\text{A2})$$

$$N_0(x) = (2/\pi)\ln(x/2), \quad N'_0(x) = 4/\pi x.$$

Substituting (A2) in (A1) gives

$$\tan\delta_{j=1/2} = \frac{-\gamma_{1/2}}{\frac{4}{r_s\pi} - \frac{2\gamma_{1/2}}{\pi} \ln\left[\frac{|E|r_s}{2p}\right]} \cong \frac{\pi}{2 \ln\left[\frac{|E|r_s}{2p}\right]}. \quad (\text{A3})$$

This is Eq. (14) in the text. As mentioned, (A3) is independent of  $\gamma_{1/2}$ , and therefore of the strength of the potential; if the potential is very weak, however, (A3) will be valid only very close to  $|E| \rightarrow 0$ .

To connect the phase shift in Eq. (A3) to the asymptotic form of  $\Delta\rho(r)$  for  $r \rightarrow \infty$  we square the wave function in Eq. (11), subtract the zero-phase-shift charge density, and make use of the asymptotic trigonometric expansions for the Bessel functions for large argument. (The details of the procedure are outlined in Ref. 6.) This leads to

$$\begin{aligned} \Delta\rho(r \rightarrow \infty) &\propto \int_0^1 \frac{1}{r} \sin[\delta_j(E)] \sin\left[\frac{2|E|r}{p}\right] dE \\ &\propto \int_0^1 \frac{1}{r} \frac{\sin\left[\frac{2|E|r}{p}\right]}{\ln\left[\frac{|E|r_s}{2p}\right]} dE, \end{aligned} \quad (\text{A4})$$

Eq. (15). The limit in the integral indicates that for  $r \rightarrow \infty$ , the largest contribution comes from very near (but not exactly)  $E = 0$ . We have used the theorem from Fourier transforms that the most severe singularity will dominate the large-argument regime of the transform; this restricts (A4) to the  $j = \frac{1}{2}$  channel, whose phase shift contains a more severe singularity in its derivative than for  $j > \frac{1}{2}$ . The leading power-law behavior of (A4) is obtained as follows. Consider  $\Delta\rho$  for a scaled argument  $\alpha r$ :

$$\Delta\rho(\alpha r) = \frac{1}{\alpha^2} \int_0^1 \frac{1}{r} \frac{\sin\left[\frac{2|E'|r}{p}\right] dE'}{\ln\left[\frac{|E'|r_s}{2p}\right] - \ln\alpha}. \quad (\text{A5})$$

If  $\alpha$  is close to unity then  $\ln\alpha$  may be ignored and (A5) becomes

$$\Delta\rho(\alpha r) \cong \frac{1}{\alpha^2} \Delta\rho(r), \quad (\text{A6})$$

which is only consistent with

$$\Delta\rho(r) \propto \frac{1}{r^2}. \quad (\text{A7})$$

Because of the  $\ln\alpha$  term in (A5),  $\Delta\rho(r)$  actually goes to zero somewhat more rapidly than  $1/r^2$ ; hence we write

$$\Delta\rho(r) = -\frac{f(r)}{r^2}, \quad (\text{A8})$$

Eq. (16) in the text. Since (A8) must be integrable,  $f(r)$  must go to zero for  $r \rightarrow \infty$ ; however, it must go more slowly than any power law. A numerical determination of  $f(r)$  can also be made by evaluating (A4) by steepest descents, with the saddle point of the integration lying on the imaginary energy axis.

The construction of the asymptotic behavior of  $\Delta\rho(r)$  in the Thomas-Fermi theory proceeds rather differently, although the result is essentially the same. Let us suppose that both  $\Delta\rho(r)$  and  $U_2(r)$  obey some asymptotic power law:

$$\Delta\rho(r) \sim \frac{1}{r^n} \quad (\text{A9})$$

$$U_2(r) \sim \frac{1}{r^m}.$$

One relation between  $n$  and  $m$  is provided by Eq. (24). It says that  $\Delta\rho \propto (U_2)^2$ ; therefore,  $n = 2m$ . A second relation is given by the Poisson equation, which relates  $\Delta\rho$  and  $U$  in Eq. (22).  $\Delta\rho(q)$  is defined by

$$\begin{aligned} \Delta\rho(q) &= \int d\vec{r} \Delta\rho(\vec{r}) e^{i\vec{q}\cdot\vec{r}} \\ &= 2\pi \int_0^\infty dr r \Delta\rho(r) J_0(qr). \end{aligned} \quad (\text{A10})$$

To obtain  $\Delta\rho(q)$  for small  $q$  (but sufficiently large enough so that  $qr > 1$ ) we insert the asymptotic expression for  $J_0$  and obtain

$$\Delta\rho(q) \sim q^{n-2} \quad (\text{A11})$$

when  $\Delta\rho(r) \sim r^{-n}$ . By Eq. (24),  $U_2^H$  is

$$U_2^H(r) \propto \int e^{-i\vec{q}\cdot\vec{r}} \frac{\Delta\rho(q)}{|\vec{q}|} d\vec{q} \propto \int_0^\infty dq \Delta\rho(q) J_0(qr). \quad (\text{A12})$$

By the same approximation as above, this leads to

$$U_2^H \sim r^{-n+1}. \quad (\text{A13})$$

So  $m = 1 - n$ . This and the condition  $n = 2m$  are satisfied

only if  $n=2$ ,  $m=1$ . [Note that the external potential  $U_2^{\text{ext}}$  in Eq. (21) also contributes a  $1/r^1$  part to the total potential, and so is consistent with the above conclusion.] We therefore find, as in the effective-mass theory, that the leading power-law dependence of  $\Delta\rho$  is  $1/r^2$ . Of course,  $\Delta\rho$  must be integrable, which leads us to our final form for  $\Delta\rho$  [Eq. (25)]:

$$\Delta\rho(r) = \pm \frac{g(r)}{r^2}, \quad (\text{A14})$$

where  $g(r)$  goes to zero as  $r \rightarrow \infty$  more slowly than any power of  $r$ . It cannot be determined from the present analysis if  $g(r)$  in Eq. (A14) and  $f(r)$  in the effective-mass theory [Eq. (A8)] are related.

- <sup>1</sup>J. W. Milliken and J. E. Fischer, *J. Chem. Phys.* **78**, 5800 (1983).
- <sup>2</sup>R. S. Markiewicz, *Ordering in Two Dimensions* (North-Holland, Amsterdam, 1981), p. 399.
- <sup>3</sup>S. B. DiCenzo, S. Basu, G. K. Wertheim, D. N. E. Buchanan, and J. E. Fischer, *Phys. Rev.* **25**, 620 (1982); S. B. DiCenzo, S. Basu, and G. K. Wertheim, *Synth. Met.* **3**, 139 (1981); S. B. DiCenzo, G. K. Wertheim, S. Basu, and J. E. Fischer, *Phys. Rev. B* **24**, 2270 (1981).
- <sup>4</sup>L. A. Grunes and J. J. Ritsko, *Phys. Rev. B* **28**, 3439 (1983).
- <sup>5</sup>A. D. Boardman and D. G. Graham, in *The Physics of Semimetals and Narrow-gap Semiconductors*, edited by D. L. Carter and R. T. Bates (Pergamon, Oxford, 1971), p. 149.
- <sup>6</sup>L. Liu and C. Verie, *Phys. Rev. Lett.* **37**, 453 (1976); L. Liu and D. Brust, *Phys. Rev.* **173**, 777 (1968); **157**, 627 (1967).
- <sup>7</sup>S. T. Pantelides, *Rev. Mod. Phys.* **50**, 797 (1978).
- <sup>8</sup>L. Pietronero, S. Strassler, H. R. Zeller, and M. J. Rice, *Phys. Rev. Lett.* **41**, 763 (1978); *Solid State Commun.* **30**, 399 (1979); S. A. Safran and D. R. Hamann, *Phys. Rev.* **22**, 606 (1980).
- <sup>9</sup>N. A. W. Holzwarth, S. G. Louie, and S. Rabii, *Phys. Rev. B* **28**, 1013 (1983); N. A. W. Holzwarth, L. A. Girifalco, and S. Rabii, *ibid.* **18**, 5206 (1978).
- <sup>10</sup>J. M. Luttinger and W. Kohn, *Phys. Rev.* **97**, 869 (1955).
- <sup>11</sup>G. S. Painter and D. E. Ellis, *Phys. Rev. B* **1**, 4747 (1970).
- <sup>12</sup>J. Callaway, *Quantum Theory of the Solid State* (Academic, New York, 1974), p. 373.
- <sup>13</sup>Ref. 12, p. 410.
- <sup>14</sup>Eugen Merzbacher, *Quantum Mechanics*, 2nd ed. (Wiley, New York, 1970), p. 270.
- <sup>15</sup>J. J. Sakurai, *Advanced Quantum Mechanics* (Addison-Wesley, Reading, Massachusetts, 1978), p. 80.
- <sup>16</sup>An interesting parallel discussion of the three-dimensional Dirac equation in a system with cylindrical symmetry may be found in F. Gesztesy and L. Pittner, *J. Phys. A* **11**, 679 (1978).
- <sup>17</sup>C. Kittel, *Quantum Theory of Solids* (Wiley, New York, 1963), p. 342.
- <sup>18</sup>Ref. 7, p. 812.
- <sup>19</sup>The actual total potential at all points in the C plane after the introduction of the impurity is accurately given by  $V_{\text{tot}}(r) = -U_2(r) + V_{\text{crystal}}^0(r)$  within the effective-mass approximation. The potential of Eq. (20) represents the change in the potential caused by the defect. The polarization of the underlying crystal charge density, which would modify the second term in the equation above and would add additional high Fourier components to Eq. (20), is a higher-order effect and will not be considered here.
- <sup>20</sup>M. Candel, *Comp. Phys. Comm.* **23**, 343 (1981).
- <sup>21</sup>G. Campagnoli and E. Tosatti, *J. Phys. C* **15**, 1457 (1982).
- <sup>22</sup>K. Kume, Y. Maniwa, H. Suematsu, Y. Iye, and S. Tamuma, *Proceedings of the Third International Conference on Graphite Intercalation Compounds* (in press).
- <sup>23</sup>S. Doniach and M. Sunjic, *J. Phys. C* **3**, 285 (1970).
- <sup>24</sup>E. J. Mele and J. J. Ritsko, *Phys. Rev. Lett.* **43**, 68 (1979).
- <sup>25</sup>See, e.g., C. A. Swarts, J. D. Dow, and C. P. Flynn, *Phys. Rev. Lett.* **43**, 158 (1979); U. von Barth and G. Grossmann, *Phys. Rev. B* **25**, 5150 (1982).
- <sup>26</sup>D. P. DiVincenzo and E. J. Mele, *Phys. Rev. B* **25**, 7822 (1982).
- <sup>27</sup>D. P. DiVincenzo and E. J. Mele, *Intercalated Graphite*, edited by M. S. Dresselhaus, G. Dresselhaus, J. E. Fischer, and M. J. Moran (North-Holland, New York, 1983), p. 123.
- <sup>28</sup>P. Hawrylak and K. R. Subbaswamy, *Phys. Rev. B* **28**, 4851 (1983).